in the GDP form of Ras, the conformational changes in the switch II region appear to resemble the changes in EF-Tu where GTP binding results in the addition of an extra helical turn at the carboxyl end of $\alpha 2$ at the expense of a turn at the beginning of the helix[12]. In conjunction with this, the $\alpha 2$ helix rotates by $\sim 40^\circ$ about an axis perpendicular to the helical axis. In $G_{t\alpha}$, rather than losing a turn at the beginning and gaining a turn at the end of $\alpha 2$, the GTP-induced changes straighten out an otherwise distorted 3_{10} helix while disrupting a reverse turn at the end of the helix. Furthermore, the rotation of the helical axis seen in p21 Ras and EF-Tu is replaced by a $\sim 90^\circ$ rotation roughly parallel to (but not coincident with) the helical axis. Finally, the partial unzipping of $\beta 3$–$\beta 1$ and concomitant extension of $\beta 3$–$\beta 2$ that couples the switch I and II regions in $G_{t\alpha}$, does not occur in either Ras[8–10] or EF-Tu[12]. Most distinctive is the presence in $G_{t\alpha}$ of a set of polar and nonpolar linkages that couple the primary structural changes, induced by interaction with the γ-phosphate, to nearby surface elements, some of which have been implicated in interactions with other components of the signalling system. Because these linkages are formed by residues that are unique to and conserved in G_α subunits we suggest that they provide the basis for a common switch mechanism in heterotrimeric G-protein-coupled signal transduction. □

Received 18 April; accepted 12 May 1994.

1. Hepler, J. R. & Gilman, A. G. *Trends Biochem. Sci.* **17,** 383–387 (1992).
2. Simon, M. I., Strathmann, M. P. & Gautam, N. *Science* **252,** 802–808 (1991).
3. Conklin, B. R. & Bourne, H. R. *Cell* **73,** 631–641 (1993).
4. Hurley, J. B. *J. Bioenerg. Biomembranes* **24,** 219–226 (1992).
5. Pfister, C. *et al. Cell Sig.* **5,** 235–241 (1993).
6. Hargrave, P. A. & Hamm, H. E. in *Molecular Pharmacoloy of Cell Regulation* Vol. 3 (eds Sibley, D. R. & Houslay, M. D.) 25–67 (Wiley, New York, 1994).
7. Bourne, H. R., Sanders, D. A. & McCormick, F. *Nature* **348,** 125–132 (1990).
8. Pai, E. F. *et al. Nature* **341,** 209–214 (1989).
9. Brunger, A. T. *et al. Proc. natn. Acad. Sci. U.S.A.* **87,** 4849–4853 (1990).
10. Tong, L. *et al. J. molec. Biol.* **217,** 503–516 (1991).
11. Jurnak, F. *Science* **230,** 32–36 (1985).
12. Berchtold, H. *et al. Nature* **365,** 126–132 (1993).
13. Noel, J. P., Hamm, H. E. & Sigler, P. B. *Nature* **366,** 654–663 (1993).
14. Mazzoni, M. R., Malinski, J. A. & Hamm, H. E. *J. biol. Chem.* **266,** 14072–14081 (1991).
15. Sternweis, P. C. & Gilman, A. C. *Proc. natn. Acad. Sci. U.S.A.* **79,** 4888–4891 (1982).
16. Fung, B. K.-K. & Nash, C. R. *J. biol. Chem.* **258,** 10503–10510 (1983).
17. Mazzoni, M. R. & Hamm, H. E. *J. Prot. Chem.* **12,** 215–221 (1993).
18. Higashijima, T. *et al. J. biol. Chem.* **262,** 752–756 (1987).
19. Faurobert, E. *et al. EMBO J.* **12,** 4191–4198 (1993).
20. Miller, R. T. *et al. Nature* **267,** 712–715 (1988).
21. Lee, E., Taussig, R. & Gilman, A. G. *J. biol. Chem.* **267,** 1212–1218 (1992).
22. Clark, K. L., Dignard, D., Thomas, D. Y. & Whiteway, M. *Molec. cell. Biol.* **13,** 1–8 (1993).
23. Whiteway, M. *et al. Molec. cell. Biol.* (in the press).
24. Thomas, T. C., Schmidt, C. J. & Neer, E. J. *Proc. natn. Acad. Sci. U.S.A.* **90,** 10295–10298 (1993).
25. Rarick, H. M., Artemyev, N. O. & Hamm, H. E. *Science* **256,** 1031–1033 (1992).
26. Berlot, C. H. & Bourne, H. R. *Cell* **68,** 911–922 (1992).
27. Stryer, L., Hurley, J. B. & Fung, B. K.-K. *Meth. Enzym.* **96,** 617–627 (1983).
28. Brunger, A. T. *Acta. crystallogr.* A**46,** 46–57 (1990).
29. Brunger, A. T. *X-PLOR Version 3.1 Manual* (Yale University, 1993).
30. Jones, T. A. *et al. Acta crystallogr.* A**47,** 110–119 (1991).
31. Jones, T. A. *J. appl. Crystallogr.* **11,** 268–276 (1978).
32. Yatsunami, K. & Khorana, H. G. *Proc. natn. Acad. Sci. U.S.A.* **82,** 4316–4320 (1985).
33. Robishaw, J. D. *et al. Proc. natn. Acad. Sci. U.S.A.* **83,** 1251–1255 (1986).
34. Nukada, T. *et al. FEBS Lett.* **197,** 305–308 (1986).
35. Van Meurs, K. P. *et al. Proc. natn. Acad. Sci. U.S.A.* **84,** 3107–3111 (1987).
36. Strathmann, M. & Simon, M. I. *Proc. natn. Acad. Sci. U.S.A.* **87,** 9113–9117 (1990).
37. Fong, H. K. W., Yoshimoto, K. K., Eversole-Cire, P. & Simon, M. I. *Proc. natn. Acad. Sci. U.S.A.* **85,** 3066–3070 (1988).
38. Nakafuku, M., Itoh, H., Nakamura, S. & Kaziro, Y. *Proc. natn. Acad. Sci. U.S.A.* **84,** 2140–2144 (1987).
39. Capon, D. J., Chen, E. Y., Levinson, A. D., Seeburg, P. H. & Goeddel, D. *Nature* **302,** 33–37 (1983).
40. Laursen, R. A., L'Italien, J. J., Nagarkatti, S. & Miller, D. L. *J. biol. Chem.* **256,** 8102–8109 (1981).
41. Fawzi, A. B. & Northrup, J. K. *Biochemistry* **29,** 3804–3812 (1990).
42. Higashijima, T. *et al. J. biol. Chem.* **262,** 762–766 (1987).
43. John, J., Frech, M. & Wittinghofer, A. *J. biol. Chem.* **263,** 11792–11799 (1988).
44. Kjeldgaard, M. & Nybord, J. *J. molec. Biol.* **223,** 721–742 (1992).

ACKNOWLEDGEMENTS. We thank R. Sweet and L. Berman of the Brookhaven National Lab for access to and help with the X-25 beam line at the NSLS, G. van Duyne, J. Geiger, J. Sondek and G. Ghosh for assistance during data collection, and C. Berlot, N. Artemyev and H. Dohlman for discussion. This work was supported by grants from the NIH to P.B.S. and H.E.H. H.E.H. was also supported by the American Heart Association and Research to Prevent Blindness. D.G.L. was a Damon Runyon postdoctoral fellow and J.P.N. was a NSF Chemistry and NIH postdoctoral fellow. The coordinates of $G_{t\alpha}$·GDP will be submitted to the Protein Data Bank.

Dust depletion in the inner disk of β Pictoris as a possible indicator of planets

P. O. Lagage & E. Pantin

C.E.A., DSM, DAPNIA, Service d'Astrophysique, C.E. Saclay, F-91191 Gif-sur-Yvette Cédex, France

IT is not yet possible to see planets orbiting other stars, although this may soon change as observing methods improve[1]. Indirect evidence for the presence of circumstellar dust disks out of which planets could form has been obtained for several stars, in the form of excess infrared emission, presumed to be from the hot dust[2,3]. Planets orbiting in such dust disks would be expected to sweep out dust-free tracks[4]. Indirect evidence for dust-free regions has been reported[5–9], based on an analysis of the spectral energy distribution, but the interpretation of the observation is not unique[7,9]. Here we present an infrared image of the inner dust disk of the star β Pictoris with a linear resolution of 5 astronomical units (AU), equivalent to the distance from the Sun to Jupiter. We find that the dust is asymmetrically distributed and is clearly depleted within 40 AU of the star, which we interpret as indicating the possible presence of at least one planetary body orbiting β Pictoris.

The 10-μm region is one of the best spectral ranges to achieve high angular resolution for an object like the β Pictoris disk. The outer part of the disk (>100 AU) has been first imaged with ground-based observations in the visible part of the spectrum[10]. But because of too high a contrast between the star and the disk emission, the disk structure within 2.5 arcsec of the star (40 AU at the distance of β Pictoris, 16 pc) has been inaccessible until now, even with sophisticated techniques such as coronagraphic optics or anti-blooming CCDs (charge-coupled devices)[11,12]. Observing at 10 μm alleviates this problem, because the thermal emission from dust is comparable in intensity to the photospheric emission of the star, while the diffraction-limited angular resolution is still high: 0.7 arcsec for a 3-m telescope. This resolution, which has not been achieved with either single detectors or with arrays of discrete detectors[8,9] is now accessible with the new generation of integrated detector arrays. The European Southern Observatory (ESO) has recently acquired an instrument that employs such a device: the TIMMI camera, built by the Service d'Astrophysique at Saclay[13]. The detector is a monolithic 64 × 64 gallium-doped silicon array hybridized by indium bumps to a direct read out circuit, optimized by the LIR (Laboratoire Infra-Rouge) at the Grenoble Centre d'Etudes Nucléaires for the high-background conditions of ground-based broad-band imaging. The TIMMI camera mounted on the 3.6-m telescope at the ESO, La Silla, Chile was used during five nights (6–11 January 1993) for imaging the β Pictoris dust disk at sub-arcsec resolution.

The disk structure observed after an on-source integration time of 75 min (spread over three nights) with a pixel field of view of 0.3 arcsec and a 10.5–13.3 μm band-pass filter is shown in Figs 1 (main figure) and 2; the signal-to-noise ratio at the

peak is ~100. The weather was good during the observations, and the air-mass was always below 1.3. The photometry was done using the nearby (5°) star α Carinae; a total (star + disk) flux of 2.28 Jy was found within an equivalent beam diameter of 4 arcsec (before deconvolution), in agreement with previous measurements[14,15]. The star α Carinae was also used to determine the point-spread function (the smearing of light by the atmosphere and the instruments) and to subtract the β Pictoris stellar contribution (the scaling factor between the two stars was taken to be 0.0111, ref. 14). The disk contribution is large (always >40% of the total flux), so that removing the stellar contribution is not critical; the uncertainty in the removed part is 20% in each pixel (see legend of Fig. 2), whereas the central disk contribution would be hidden only for uncertainties greater than 60%. To go beyond the angular resolution limitation imposed by the point-spread function (full-width half-maximum of ~0.9 arcsec), we used the Richardson–Lucy deconvolution technique[16,17] combined with wavelet filtering[18], which prevents noise amplification. We monitored the point-spread function by interleaving the observations of β Pictoris with observations of the two nearby ESO catalogue reference stars, α Carinae and γ Reticuli. The latter star was used to determine the residuals of the deconvolution method (see Fig. 1, inset).

Fig. 1 confirms without ambiguity the previous claims that the β Pictoris dust disk is extended at 10 μm (refs 8, 9); the emission extends to more than 4 arcsec from the star. The second striking feature directly seen in the image is the asymmetric morphology of the disk. Neither property is an artefact of the data

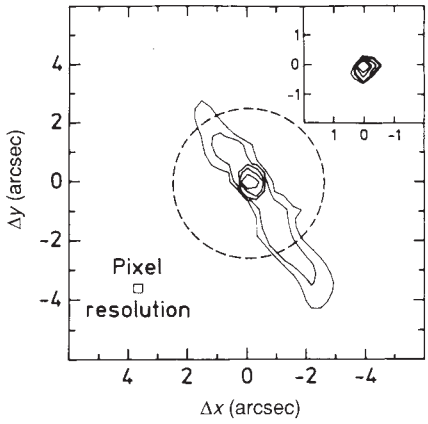

FIG. 1 Main figure, the deconvoluted β Pictoris dust disk, (the star contribution has been removed), as seen at 11.9 μm with a spatial resolution of 0.3 arcsec (5 AU at the distance of the object). The highest contour corresponds to 1.2 Jy arcsec^{-2}, at each subsequent contour the flux is divided by 3. North is top; east is left. The usual chopping and nodding technique was used to remove the atmosphere and telescope background contribution. The secondary chopping mirror unit of 3.6 m ESO telescope was used at a frequency of 5 Hz; changes of telescope position (nodding) was done every 40 s. The total on-source integration time (half of the total time) was 75 min. The region inside the dashed circle (2.5-arcsec radius) was inaccessible to previous observations in visible radiation. A broad-band filter (10.5–13.3 μm) was used. The large well depth of the detectors (~3×10^7 electrons per pixel) allows the use of broad-band filters without saturation by the huge photon background emitted at 10 μm by the telescope and the atmosphere. These detectors are a by-product of the detector development programme undertaken for ISOCAM, an imaging instrument to be installed on the Infrared Space Observatory (ISO)[25]. Inset, Result of deconvolution of two reference stars, α Carinae and γ Reticuli, showing that the residuals after deconvolution are at a low level; (The flux is divided by 3 between adjacent contours, as on the main Figure). These residuals are conservative because γ Reticuli is much farther away from α Carinae than β Pictoris (30° instead of 5°), so that aberrations dependent on the telescope position are included in the residuals.

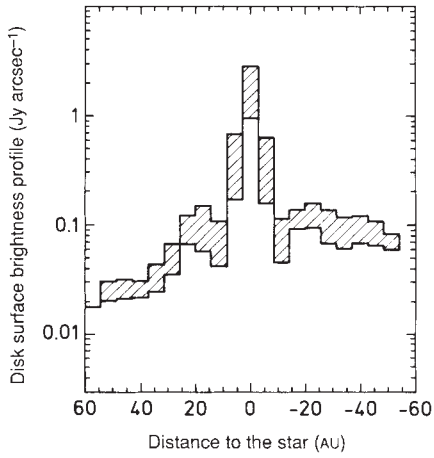

FIG. 2 Surface brightness profile of the disk integrated over 3 pixels perpendicular to the disk plane (in order to avoid sampling errors due to the fact that the disk is not aligned with the array; the flux outside these 3 pixels is negligible), as a function of the distance to β Pictoris (east is positive) in astronomical units (1 arcsec = 16 AU). Half of the flux is in the central bin, 70% is in the three central bins. The shaded region corresponds to conservative uncertainties in the process of star-contribution removal and deconvolution. The photometric error over a beam with a diameter of 9 pixels and extending over the two-dimensional image was measured to be ±7% (peak-to-peak variation for 10 measurements). If we also consider sampling errors, we obtain ±15% on a pixel (peak-to-peak variation of the central pixel for 10 measurements). Finally, we have taken an uncertainty of ±20% in the β Pictoris stellar contribution, which includes an additional uncertainty of 5% on the scaling factor between α Carinae and β Pictoris. In reality these uncertainties are too conservative. As the observations of α Carinae have been interspersed with the observations of β Pictoris, we were able to monitor the time variations in the photometry and point spread function (PSF). The sampling error has also been overestimated, because co-adding several observations of the same object obtained at various positions on the array averages the sampling error, and decreases the difference between the sampling of the object and of the reference star. We have also overestimated the uncertainties of the PSF variation with the telescope position, by adding linearly the uncertainties obtained when using γ Reticuli (30° away from β Pictoris) instead of α Carinae (5° away from β Pictoris).

analysis, as each is already visible in the raw data. To obtain the dust density profile, some modelling is necessary, because the observed surface brightness also depends on the grain temperature T, on the grain absorption coefficient Q_{abs} and on the grain size distribution. Furthermore, as the disk is seen edge-on[10] and asymmetric, we can only derive directly from the observations the mean surface density of the face-on disk. An estimate of the dust absorption coefficient, size distribution and temperature can be made, because we know the heat source (an A star at 8,200 K and of 6.5 solar luminosity) and the nature of some of the particles (silicate grains, as shown by the detection in a 5 arcsec beam of the silicate feature near 10 μm[14,15,19]). The derived profile of the mean surface density is shown in Fig. 3 (see Fig. legend for details of the calculations). We conclude that there is no strict void of matter near the star, but rather a relatively steep decrease of the mean density when approaching it.

The density distribution inferred for the inner region is quite different from that in the outer region (>100 AU) deduced from visible observations[7,10]. The beginning of a transition region has been observed at ~100 AU by recent visible observations which can distinguish structures farther than 40 AU from the star[11,12], which is further than the size of Pluto's orbit. This transition is attributed to the sublimation of ice particles, as supported by the

two-component models of ref. 9. Given the strong dependence of the sublimation timescale on the dust temperature[20], the transition region should not be very large (a few tens of AU at most), so that we do not expect this mechanism to be able to reproduce the density decrease observed within 30 AU, except if the dust particles had a high eccentricity. On the other hand, planets are able to produce a steep deficiency of matter in this region; the matter can be either swept up by the planet[10], or trapped in gravitational resonances induced by the planet (for example, ref. 21). Given the age of the β Pictoris system ($(1–2)\times10^8$ yr), planets could have formed up to a maximum radius of ~20 AU (the size of Uranus' orbit), according to Nakano[22], but the models of planet formation are still uncertain. Detailed calculations of the effect of planets on a dust disk, taking into account gravitation and Poynting–Robertson effects but neglecting particle collisions, have been presented recently[21]. These models show that planets with masses as low as a few Earth masses are able to produce a large depletion of matter inside their orbit on a timescale of 10^5–10^6 yr. The density predicted by these models agrees with the observations in the 10–30 AU region, but the predicted profile is too steep inside 10 AU (Fig. 3). Particle collisions may help in filling the innermost region.

Another possibility is the direct injection of particles into the innermost region (<3 AU) by comet evaporation, although this was introduced in a completely different context: the interpretation of the redshifted and variable gaseous absorption lines observed in the visible and ultraviolet radiation[23]. A total of 1,000 comets per year, each a kilometre in size, is required to explain the observations[24]; these would give rise to a dust inflow rate of $\sim5\times10^{18}$ g yr^{-1}. Evidence that the inner 10-μm emission could originate from cometary materials is provided by the shape of the silicate feature observed at 10 μm (refs 13, 14, 19). The total dust-mass necessary to account for the 10-μm observations of the innermost region presented here is $\sim6\times10^{20}$ g. The associated dust flow varies between 6×10^{17} g yr^{-1} to 6×10^{20} g yr^{-1} according to the dust removal process under consideration; (radiation pressure which rapidly blows out small particles or Poynting–Robertson effect which makes the particles slowly fall onto the star). Comets therefore are possible candidates as sources of replenishment of the innermost region observed here.

If a planet is present near β Pictoris, its orbit is probably eccentric, as are most of the planetary orbits in our Solar System. A planet with even a moderate eccentricity of 0.02 should generate a spectacular asymmetry, such as arc-like structures[21] in the dust disk. In this context, the asymmetry observed here can be considered as more evidence in favour of the presence of a planet near β Pictoris. Such an asymmetry should vary in time, and it would be interesting to monitor. Some patience may be required, however, because the half-orbital period of an object 20 AU from the central star is 36 years. □

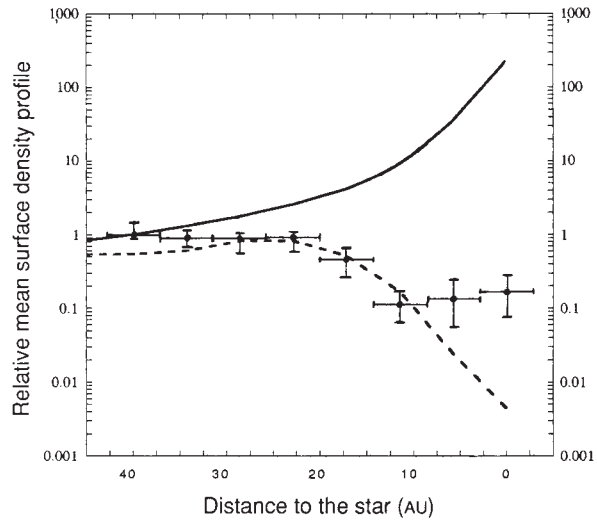

FIG. 3 Profile (crosses) of the face-on surface-density averaged along the line of sight, l, responsible for the observed flux of Fig. 2, S_{obs}, at an angular distance θ from the star in the disk direction perpendicular to the line of sight. (We do not consider a volume density as we have integrated the observed flux over the direction perpendicular to the disk plane.) $B_\lambda(T)$ is the blackbody brightness, $N(a)da$ is the probability of having particles with sizes between a and $a+da$.

$$\langle n\rangle_{obs}(\theta)=S_{obs}(\theta)/[\int_{-\infty}^{\infty}\int_{sizedist.}\int_{filter}\pi a^2 Q_{abs}(a)B_\lambda(T(r,a))N(a)(D^{-2})\,dl\,da\,d\lambda] \quad (1)$$

(the radial coordinate r is related to θ and l via the usual relation $r=\sqrt{l^2+\theta^2\times D^2}$, where D is the β Pictoris–earth distance). We have assumed silicate grains with an absorption coefficient Q_{abs} taken from ref. 26 and a size distribution as in[19] ($N(a)=9.8a^{-2}$ μm^{-1} with a cut-off and a cut-on, respectively, at 0.1 μm and 5 μm) and independent of the distance to the star r. Such a distribution (flatter than usual) has also been found in another main-sequence star with an infrared excess, HD98800 (ref. 27). The particle-size dependence of the radiation pressure (small particles are rapidly blown out of the system) may explain the flatness of the distribution. The profile has been limited to 40 AU, because at greater distances the uncertainties due to the modelling entering in equation (1) become significant, given that the calculated temperature (<100 K) is far from 300 K, the temperature for which the emission peaks at 10 μm. Note that even if the observed brightness keeps on increasing towards the star (Fig. 2), the density profile must decrease to compensate for the strong increase in the dust temperature near the star. The density in the central part is 3×10^8 particles m^{-2}. The observations are compared with two models. The solid line represents the profile expected for a radial density following a $r^{-1.7}$ law (outer-region density integrated upon the disk thickness). The dotted line represents the dust profile expected if a planet was at 20 AU according to the model calculations of ref. 21.

Received 30 December 1993; accepted 13 May 1994.

1. Angel, J. R. P. *Nature* **368,** 203–207 (1994).
2. Aumann, H. H. *Publs astr. Soc. Pacif.* **97,** 885–891 (1985).
3. Backman, D. E. & Paresce, F. in *Protostars and Planets III* (eds Levy, E. H., Lumine, J. I. & Matthews, M. S.) 208–253 (Univ. Arizona Press, Tucson, 1993).
4. Paresce, F. *Adv. Space Res.* **12,** 157–167 (1992).
5. Gillett, F. C. in *Light on Dark Matter* (ed. Israel, F. P.) 61–69 (Reidel, Dordrecht, 1986).
6. Diner, D. J. & Appleby, J. F. *Nature* **322,** 436–438 (1986).
7. Artymowicz, P., Burrows, C. & Paresce, F. *Astrophys. J.* **337,** 494–513 (1989).
8. Telesco, C. M., Becklin, E. E., Wolstencroft, R. D. & Decher, R. *Nature* **335,** 51–53 (1986).
9. Backman, D. E., Gillett, F. C. & Witteborn, F. C. *Astrophys. J.* **385,** 670–679 (1992).
10. Smith, B. A. & Terrile, R. J. *Science* **226,** 1421–1424 (1984).
11. Lecavelier des Etangs, A. *et al. Astr. Astrophys.* **274,** 877–882 (1993).
12. Golimowski, D. A., Durrance, S. T. & Clampin, M. *Astrophys. J.* **411,** L41–L44 (1993).
13. Lagage, P. O. *et al.* in *Infrared Detectors and Instrumentation* Vol. 1946 (ed. Fowler, A. W.) 655–666 (SPIE, Orlando, Florida, 1993).
14. Telesco, C. M. & Knacke, R. F. *Astrophys. J.* **372,** L29–L31 (1991).
15. Aitken, D. K., Moore, T. J. T., Roche, P. F., Smith, C. H. & Wright, C. M. *Mon. Not. R. astr. Soc.* **265,** L41–L43 (1993).
16. Richardson, B. H. *J. opt. Soc. Am.* **62,** 55–59 (1972).
17. Lucy, L. B. *Astrophys. J.* **79,** 745–754 (1974).
18. Starck, J. L. & Murtagh, F. *Astr. Astrophys.* (in the press).
19. Knacke, R. F. *et al. Astrophys. J.* **418,** 440–450 (1993).
20. Isobe, S. *Publs astr. Soc. Japan* **22,** 429–445 (1970).
21. Roque, F., Scholl, H., Sicardy, B. & Smith, B. *Icarus* (in the press).
22. Nakano, T. *Mon. Not. R. astr. Soc.* **224,** 107–130 (1987).
23. Lagrange-Henri, A. M., Vidal-Madjar, A. & Ferlet, R. *Astr. Astrophys.* **190,** 275–282 (1988).
24. Ferlet, R. *et al. Astr. Astrophys.* **267,** 137–144 (1993).
25. Césarsky, C. in *Infrared Astronomy with Arrays: the Next Generation* (ed. McLean, I.) 261–268 (Astrophysics and Space Science Library Vol. 190, Kluwer Academic, Dordrecht, 1994).
26. Draine, B. T. *Astrophys. J. Suppl. Ser* **57,** 587–594 (1985).
27. Skinner, C. J., Barlow, M. J. & Justtanont, K. *Mon. Not. R. astr. Soc.* **255,** 31P–36P (1992).

ACKNOWLEDGEMENTS. P.O.L. thanks his colleagues R. Jouan, P. Masse, P. Mesteau and A. Tarrius for having built the TIMMI camera. He also thanks the staff of ESO and Service d'Astrophysique who supported the TIMMI project. We would like to thank P. Artymowicz, C. Césarsky, R. Papoular and B. Sicardy for discussions.